

Discrete multi-physics simulations of diffusive and convective mass transfer in boundary layers containing motile cilia in lungs

Ariane, Mostapha; Kassinos, Stavros; Velaga, Sitaram; Alexiadis, Alessio

DOI:

[10.1016/j.combiomed.2018.01.010](https://doi.org/10.1016/j.combiomed.2018.01.010)

License:

Creative Commons: Attribution-NonCommercial-NoDerivs (CC BY-NC-ND)

Document Version

Peer reviewed version

Citation for published version (Harvard):

Ariane, M, Kassinos, S, Velaga, S & Alexiadis, A 2018, 'Discrete multi-physics simulations of diffusive and convective mass transfer in boundary layers containing motile cilia in lungs', *Computers in Biology and Medicine*, vol. 95, pp. 34-42. <https://doi.org/10.1016/j.combiomed.2018.01.010>

[Link to publication on Research at Birmingham portal](#)

Publisher Rights Statement:

Published in *Computers in Biology and Medicine* on 01/02/2018

DOI: [10.1016/j.combiomed.2018.01.010](https://doi.org/10.1016/j.combiomed.2018.01.010)

General rights

Unless a licence is specified above, all rights (including copyright and moral rights) in this document are retained by the authors and/or the copyright holders. The express permission of the copyright holder must be obtained for any use of this material other than for purposes permitted by law.

- Users may freely distribute the URL that is used to identify this publication.
- Users may download and/or print one copy of the publication from the University of Birmingham research portal for the purpose of private study or non-commercial research.
- User may use extracts from the document in line with the concept of 'fair dealing' under the Copyright, Designs and Patents Act 1988 (?)
- Users may not further distribute the material nor use it for the purposes of commercial gain.

Where a licence is displayed above, please note the terms and conditions of the licence govern your use of this document.

When citing, please reference the published version.

Take down policy

While the University of Birmingham exercises care and attention in making items available there are rare occasions when an item has been uploaded in error or has been deemed to be commercially or otherwise sensitive.

If you believe that this is the case for this document, please contact UBIRA@lists.bham.ac.uk providing details and we will remove access to the work immediately and investigate.

Discrete multi-physics simulations of diffusive and convective mass transfer in boundary layers containing motile cilia in lungs

Mostapha Ariane^a, Stavros Kassinos^b, Sitaram Velaga^c, Alessio Alexiadis^a

^a School of Chemical Engineering, University of Birmingham, Edgbaston Birmingham B15 2TT, United Kingdom

^b Department of Mechanical and Manufacturing Engineering, University of Cyprus, 1678 Nicosia, Cyprus

^c Pharmaceutical Research Group, Division of Medical Science, Department of Health Science, Luleå University of Technology, 971 87 Luleå, Sweden

Abstract

In this paper, the mass transfer coefficient (permeability) of boundary layers containing motile cilia is investigated by means of discrete multi-physics. The idea is to understand the main mechanisms of mass transport occurring in a ciliated-layer; one specific application being inhaled drugs in the respiratory epithelium. The effect of drug diffusivity, cilia beat frequency and cilia flexibility is studied. Our results show the existence of three mass transfer regimes. A low frequency regime, which we called shielding regime, where the presence of the cilia hinders mass transport; an intermediate frequency regime, which we have called diffusive regime, where diffusion is the controlling mechanism; and a high frequency regime, which we have called convective regime, where the degree of bending of the cilia seems to be the most important factor controlling mass transfer in the ciliated-layer. Since the flexibility of the cilia

22 and the frequency of the beat changes with age and health conditions, the knowledge of these
23 three regimes allows prediction of how mass transfer varies with these factors.

24 Keywords: Discrete Multi-Physics, Smoothed Particle Hydrodynamics, Mass-Spring Model,
25 cilia, diffusivity, mass transfer

26 **1. Introduction**

27 Motile cilia are hair-like structures present on the surface of a variety of cells. They are found
28 in large numbers in the human body and beat in coordinated waves to perform a number of
29 different functions. For instance, in the conducting and central airways of the lungs, cilia are
30 surrounded by mucus that traps particulate materials and pathogens. The coordinated motion
31 of the cilia propels these materials towards the pharynx where they are swallowed or expelled
32 via coughing, a phenomenon known as mucociliary clearance or mucociliary escalator [1].
33 Mathematical modelling of this phenomenon has attracted the interest of various researchers
34 in material, biological and pharmaceutical sciences. The main motivation is to understand the
35 factors controlling the effectiveness of mucociliary clearance since this is important in the
36 context of environmental exposure (see [2] for a detailed review). [3] introduced an analytical
37 model of a mucus layer with cilia motion. Their findings suggested that the mucus flow in
38 contact with the airway is governed by a viscosity gradient in the mucus layer, but in this
39 work, the cilia were only considered as rigid rods. Later, [4] implemented a more realistic
40 cilia motion model including effective and recovery stroke in a two layers system. The
41 outcomes highlighted the role of the cilia penetration (in the mucus layer) on the mucus
42 transport effectiveness. At the beginning of the new century, [5] focused their researches on
43 the mucus draining in an idealised rigid bronchial tree with an air flow effect. Their model
44 showed the viscosity-dependence of the mucus transport as well as the important role of the

45 geometry. The emergence of the Immersed Boundary Method (IBM) has allowed a significant
46 enhancement in mucociliary clearance modelling. [6] studied the effects of the velocity, the
47 viscosity, the beat cilia frequency, the number of cilia and the depth of the periciliary layer.
48 The main results showed that (i) the velocity of the periciliary fluid is linearly proportional to
49 the cilia beat frequency, (ii) the mucus viscosity plays a little role on the mucus flow rate
50 contrary to the number of cilium which increases the mucus transport, and (iii) a minimum
51 depth of periciliary layer is needed to generate a mucociliary transport. [7] extended the two-
52 dimensional [6] model to a three-dimensional representation and thus were able to capture the
53 cilia motion in the normal direction; they confirmed the previous results. Additionally, the
54 same authors in another publication [8], focused on cilia dysfunction and malformation. They
55 emphasized the negative effects of too elastic and too rigid cilia beat patterns on the mucus
56 transport. Then, a method coupling IBM with a lattice Boltzmann method was used by [9] to
57 implement an Oldroyd-B model and to simulate a viscoelastic fluid. They found that an
58 increase of the mucus viscosity accelerates the movement of mucus layer. [10] with a penalty
59 technique, also concentrated their researches on genetic cilia diseases and defective mucus
60 clearance using a non-Newtonian model. They correlated, in the case of cystic fibrosis, mucus
61 velocity and rheology with a mucus maturation model and highlighted that shear-thinning
62 mucus can accentuate agglomeration phenomena in regions with ineffective clearance. Most
63 of the previous studies have focused on the altered effectiveness of mucociliary clearance
64 under disease states, for example in primary or acquired ciliary dyskinesia. Here, we also take
65 a look how impairments to the ciliary function can modify the speed with which pollutants,
66 irritants and toxic agents can reach the airway epithelium.

67 While mucociliary escalator is one of the major defence mechanisms protecting the lungs, it
68 has important implications in pulmonary drug delivery. In the case of inhaled aerosolized

69 medicines, mucociliary clearance competes with the particle dissolution and absorption that
70 eventually determines the lung bioavailability of the inhaled drugs [11]. Smaller particles
71 trapped in the mucus layer progressively dissolve and diffuse towards the epithelium and the
72 drug gets absorbed (Fig. 1a). On the other hand, larger or slowly dissolving particles are
73 partly cleared by the ciliary action, thus reducing the amount of drug absorbed (Fig. 1b).
74 Mucociliary clearance concerns the mass transfer of particles trapped in the mucus layer to
75 the pharynx for clearance, whilst the drug absorption depends on the diffusion of particles
76 towards the epithelium through the mucus and the ciliated-layer. The role that the cilia beat
77 pattern plays as part of the mucociliary clearance mechanism has been studied in the past.
78 While the cilia beat is also likely to affect mass transfer, to the best of our knowledge, it has
79 received no attention in the literature from this perspective.

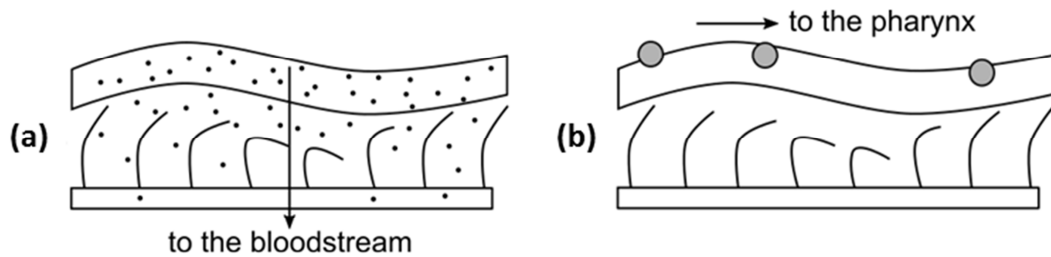


Fig. 1. Drug absorption (a) versus mucociliary clearance (b).

82 In this work, we use a modelling technique called discrete multi-physics [12-17] to investigate
83 how the motion of the cilia affects mass transfer conditions in the ciliated-layer. By means of
84 discrete multi-physics, the following research questions are addressed. Does the presence of
85 the cilia enhance or hinder the mass transfer in the ciliated layer? For example, it is known
86 that smoking, age, and health conditions affect the frequency of the cilia beat [18]. Thus, it is
87 of interest to understand how drug absorption is sensitive to the frequency of the beat. Finally,

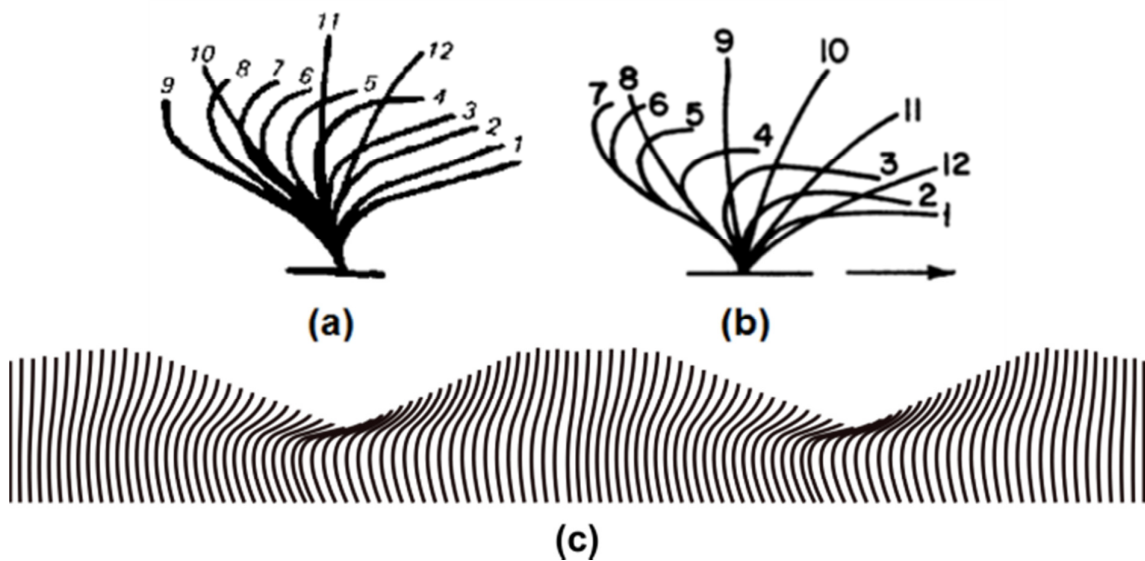
88 does the flexibility of the cilia, which also depends on age and health conditions [19], play a
89 role too?

90 Answering these questions can provide insights not only to the development of inhalation
91 medicines, or to the dynamics of harmful chemicals during environmental exposure, , but also
92 the design of artificial cilia needed for lab-on-a-chip or organ-on-a-chip applications [20].

93 **2. Preliminary considerations and background**

94 *2.1 Cilia beat*

95 In the past, several studies [21-27] have investigated the cilia motion in the respiratory
96 epithelium. The results are not always fully consistent with each other (e.g. Fig. 2), but in
97 general, the cilia motion is divided into two phases: an ‘effective stroke’, in which the cilia
98 move forward and propel the mucus layer in the same direction; and a ‘recovery stroke’, in
99 which the cilia return to their initial position.



101 Fig. 2. Cilium's motion according to (a) Sanderson and Sleigh [22] and (b) Aiello and Sleigh
102 [21] and (c) metachronal wave.

103 Moreover, the movement of each cilium (Fig. 2) is coordinated with that of the others
104 producing a wave-like overall motion known as metachronal wave. A variety of cilia beat
105 frequencies in the range between 3 and 20 Hz have been observed in the respiratory
106 epithelium, with the frequency being a function of temperature, age and health conditions [25-
107 27]. Artificial cilia used in lab-on-a-chip applications, on the other hand, can reach higher
108 frequencies in the order of 50 Hz [28].

109 *2.2 Membrane permeability and mass transfer*

110 In general, the rate of absorption of a certain drug into the body depends on the permeability
111 P_{me} [m s^{-1}] of the cellular membrane to that specific drug. In experiments, the drug's flux
112 through the membrane J [$\text{kg m}^{-2} \text{s}^{-1}$] is measured and the permeability calculated from

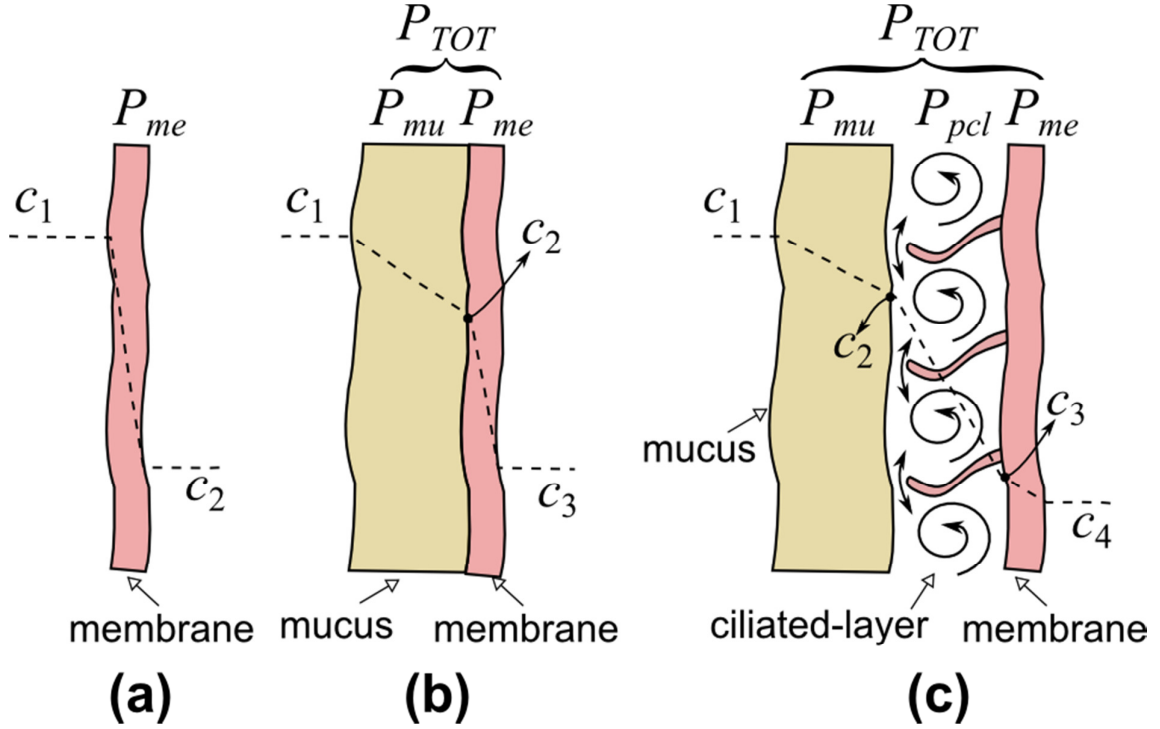
$$J = P_{me}(c_1 - c_2), \quad (1)$$

113 where $c_2 - c_1$ [kg m^{-3}] is the difference of drug's concentration across the membrane (Fig.
114 3a).

115 If before permeating the membrane, the drug diffuses through an additional mass transfer
116 resistance (e.g. the layer of mucus), the total permeability P_{TOT} of the mucus + the membrane
117 layer is given by

$$\frac{1}{P_{TOT}} = \frac{1}{P_{me}} + \frac{1}{P_{mu}}, \quad (2)$$

118 where P_{mu} is the drug's permeability of the mucus layer.



119

120 Fig. 3. Permeability through a membrane (epithelium), (b) permeability through
121 membrane + mucus, (c) permeability through membrane + mucus + ciliated-layer.

122 In the respiratory epithelium, between the mucus layer and the membrane, there is a third
123 layer, the periciliary layer (PCL), where a low-viscosity fluid is agitated by motile cilia. The
124 overall permeability of the mucus + ciliated + membrane layer is, therefore,

$$\frac{1}{P_{TOT}} = \frac{1}{P_{me}} + \frac{1}{P_{mu}} + \frac{1}{P_{pcl}}, \quad (3)$$

125 where P_{pcl} is the permeability of the ciliated-layer.

126 Permeability is the term mostly used in biology and medicine; in physics and engineering, it is
 127 often replaced by the molecular diffusivity D [$\text{m}^2 \text{s}^{-1}$], which is linked to permeability by the
 128 relation

$$P = \frac{D}{\delta}, \quad (4)$$

129 where δ [m] is the thickness of the layer where the drug diffuses. There is, however, a
 130 fundamental difference between mass transfer in the membrane or in the mucus layer, and in
 131 the PCL. The diffusivities D_{me} (membrane) and D_{mu} (mucus) originate from
 132 hydrodynamically static layers and only depend on the molecular interaction between the
 133 diffusing drug and the diffusive medium; they can be measured from standard experiments,
 134 which do not depend on hydrodynamics. The PCL, on the other hand, is hydrodynamically
 135 active since the motion of the cilia generates recirculation regions where mass transfer
 136 depends on convection rather than diffusion. Under certain conditions, discussed in Section
 137 3.2, however, the dynamics can be considered pseudo-diffusive and an apparent diffusivity
 138 coefficient D_{pcl} can be used to model the mass transport in the ciliated-layer. This means that
 139 Eq. (3) can be rewritten as

$$\frac{\delta_{TOT}}{D_{TOT}} = \frac{\delta_{me}}{D_{me}} + \frac{\delta_{mu}}{D_{mu}} + \frac{\delta_{pcl}}{D_{pcl}}, \quad (5)$$

140 While D_{me} and D_{mu} are real diffusivities, which are constant for a given drug, D_{pcl} is a
 141 pseudo-diffusivity, which also depends on the motion of the cilia. The goal of this paper is to
 142 determine how the pseudo-diffusivity D_{pcl} is affected by the three parameters: (i) the
 143 molecular diffusivity D of the drug in the periciliary fluid, (ii) the frequency f [s^{-1}] of the cilia

beat, and (iii) the flexibility of the cilia measured as bending length s [m] covered by the cilia during bending.

2.3 Soluble versus insoluble particles

Inhalation devices deliver medicines to the airways in the form of fine solid particles (typically in the range of 2 to 6 μm) or liquid droplets (aerosols). Particles that dissolve in the mucus gradually diffuse and reach the epithelium (Section 2.2). As discussed earlier, the fate of insoluble particles depends on their size. Particles larger than 6 μm are trapped in the mucus layer and eliminated by mucociliary clearance. Particles smaller than 6 μm , instead, can penetrate the mucus layer and diffuse similarly to molecules of soluble drugs. Their diffusivity D_B is the result of Brownian motion and can be calculated according to the Stokes-Einstein relation

$$D_B = \frac{k_B T}{3\pi\mu a}, \quad (6)$$

where k_B is the Boltzmann constant [$\text{kg m}^2 \text{s}^{-2} \text{K}^{-1}$], T [K] the temperature, μ [Pa s] the viscosity of the fluid and a [m] the diameter of the particle. Based on Eq. (6), in our analysis, we can treat soluble particles and small insoluble particles in the same way. The only difference being that the latter case requires the Brownian diffusivity D_B instead of the molecular diffusivity D .

3. Modelling Approach

162 To determine how the pseudo-diffusivity D_{pcl} depends on the molecular diffusivity, the beat
 163 frequency and the flexibility of the cilia, we use a computational approach called Discrete
 164 Multi-Physics (DMP) that links various discrete (i.e. particle based) modelling techniques in
 165 order to reach results not attainable with each technique separately. This method has been
 166 successfully tested for both solid-liquid flows [12-14] and fluid-structure interaction [15-17].
 167 In this study, Smoothed Particle Hydrodynamics (SPH) is used to simulate the fluid, and the
 168 Mass-Spring Model (MSM) to simulate the membrane. A brief introduction to SPH and MSM
 169 is given in Appendix A and more details can be found in the aforementioned publications.

170 *3.1 Geometry*

171 Many modelling works on mucociliary clearance follows a 2D representation of the ciliated-
 172 layer (see [2] for a review); in this study, we also follow this approach. The computational
 173 domain (Fig. 4a) is divided into four regions: the mucus, the PCL, the cilia and the membrane.
 174 SPH particles are used to model the mucus and the PCL, MSM particles are used to model the
 175 cilia, while static SPH particles are used for the membrane. In the following, we refer to the
 176 particles used for the cilia as cilia-particles, to the particles used to model the mucus layer as
 177 mucus-particles, and so on. The computational box is shown in Fig. 4b. There are 36 cilia
 178 with length $L_{pcl} = 5 \mu\text{m}$ each, the distance between cilia is $l = 0.5 \mu\text{m}$ and the total length of
 179 the section investigated is $W = 20 \mu\text{m}$; since periodic boundary conditions in the x -direction
 180 are considered, each particle whose position is $x < 0$ or $x > W$ is reintroduced on the other side
 181 of the computational box. The actual computational domain, therefore, is defined as an
 182 infinite replica in the x -direction of the computational box illustrated in Fig. 4b. The thickness
 183 of the mucus layer in the simulation is $H_{mu} = 2 \mu\text{m}$, which is lower than the actual mucus layer
 184 (typically 3-5 μm [29]). In this study, this is not a limitation since we are mostly interested in

185 the mass transport in the PCL and the mucus layer is only needed to determine the
186 concentration at the boundary conditions. A smaller mucus layer requires less computational
187 particles and allows faster simulations.

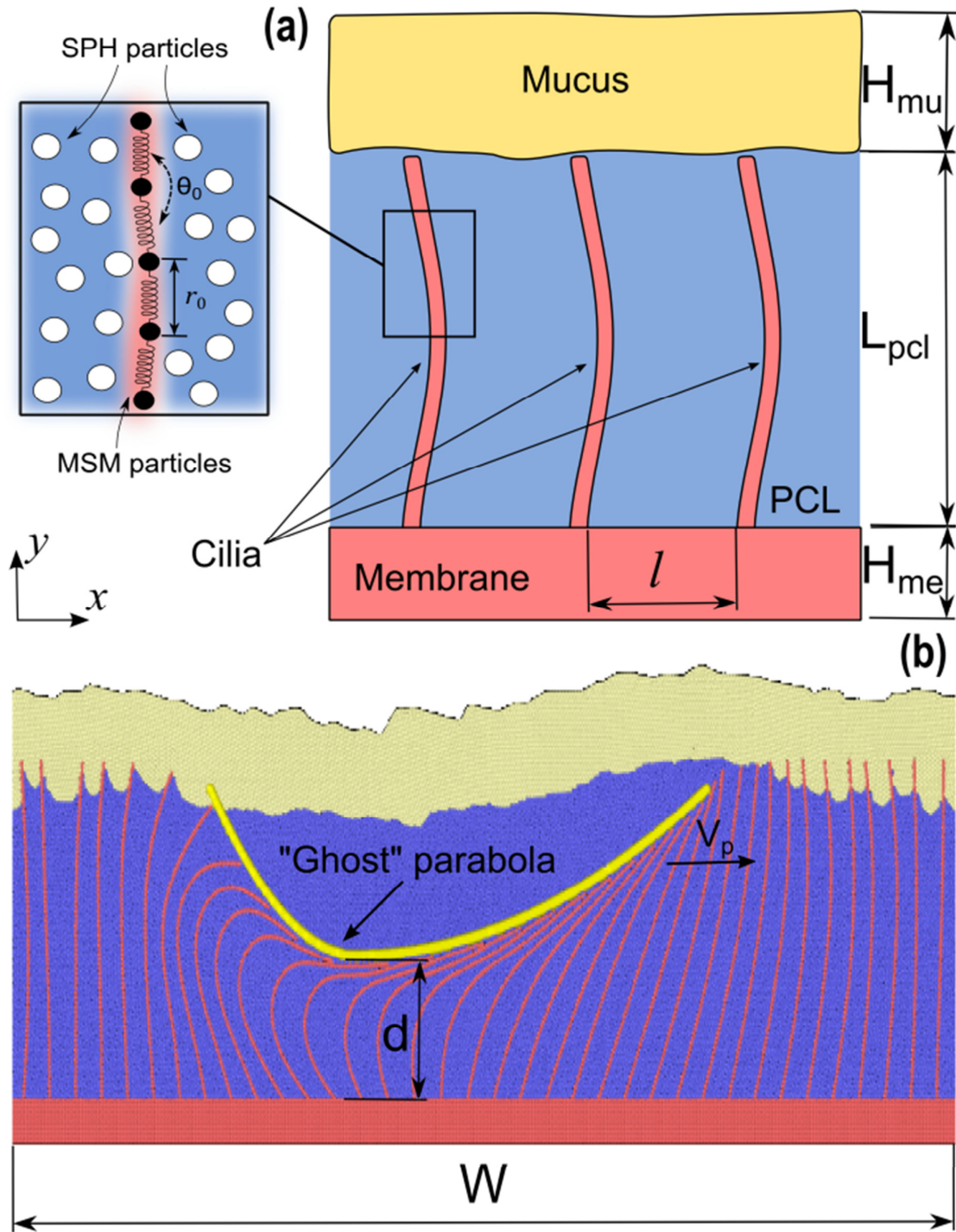


Fig. 4. The geometry of the PCL (a) and the computational box used in the simulations (b).

190 Modelling the *metachronal wave* of the cilia turned out to be a challenging task. If only a few
 191 cilia are considered, a series of time-dependent forces can be imposed to the cilia-particles
 192 resulting in an approximately correct bending and straitening motion of each cilium. When
 193 the number of cilia is above four or five, however, the interaction with the fluid produces a
 194 gradual loss of coordination among the cilia that, as time progresses, breaks the metachronal
 195 rhythm. We have tried a number of different strategies (based on forces applied to the cilia
 196 computational particles) to overcome this problem; the best solution we found consists of
 197 using a fifth type of ‘ghost’ particles that only interact, by means of a repulsive force (see
 198 Appendix A), with the cilia. These particles are arranged in a parabolic shape that moves
 199 horizontally (see Fig. 4b). The PCL fluid and the mucus do not feel the presence of these
 200 ‘ghost’ particles (no interaction forces), but if the parabola comes into contact with a cilium,
 201 the cilium bends and follows the outline of the parabola (interaction forces). When the
 202 parabola moves away, the cilium gradually recovers its original shape. In this way, the
 203 coordination of the *metachronal wave* is maintained for the entire duration of the simulation
 204 and the shapes obtained are consistent with those observed in the literature (Fig. 2). Given the
 205 periodic boundary conditions explained above, when the parabola exits the domain from $x =$
 206 W , it is re-introduced at $x = 0$. The velocity of the parabola v_p and the length of the domain W
 207 determine the frequency of the beat (i.e. $f = v_p/W$). The ‘ghost’ parabola is also used to
 208 investigate the effect of the flexibility of the cilia. During their motion, the cilia periodically
 209 bend and straighten and the degree of bending is an indication of how flexible the cilia are. By
 210 varying the distance d between the minimum of the parabola and the epithelium (Fig. 4b) we
 211 can vary the bending length and simulate cilia with different flexibilities. In the rest of the
 212 article, we refer at the distance $s = L_{pcl} - d$ as the bending length.

213

214 *3.2 Dimensionless analysis*

215 Our aim is to determine how the pseudo-diffusivity D_{pcl} depends on D , f and s . Dimensionless
216 analysis indicates that the system can be described by only two dimensionless groups. The
217 Sherwood number is defined as

$$Sh = \frac{D_{pcl}}{D}, \quad (7)$$

218 which expresses the ration between the molecular and the apparent diffusivity; and the Péclet
219 number that, here, works as a dimensionless frequency

$$Pe = \frac{s^2 f}{D}. \quad (8)$$

220 In our results, therefore, we seek correlations of the type

$$Sh = KPe^n, \quad (9)$$

221 where K and n are two constants to be determined from the simulation data.

222 In the following sections, we will also use the geometric ratio

$$\lambda = \frac{s}{L_{pcl}}, \quad (10)$$

223 which is not a fundamental dimensionless group, but it will be used, during the discussion, to
224 highlight some specific aspects that depend on the cilia flexibility.

225

226 **4. Results and discussion**

227 There are two types of parameters required for the simulations: model parameters and
228 simulation parameters. Model parameters define the SPH, MSM and DMP structures and are
229 fixed in all the simulations (Appendix B). Simulation parameters such as D , f and s , represent
230 the operative conditions and are varied as indicated in Table 1.

231

Table 1. List of simulations with diffusivities, frequencies and bending lengths parameters.

Case	D [$\text{m}^2 \text{s}^{-1}$]	f [Hz]	s [μm]	λ [-]	Pe [-]	D_{PCL} [$\text{m}^2 \text{s}^{-1}$]	Sh [-]
D10v05H3	$1 \cdot 10^{-10}$	2.5	1.3	0.27	0.04	$3.08 \cdot 10^{-11}$	0.31
D10v05H4	$1 \cdot 10^{-10}$	2.5	1.9	0.38	0.09	$3.00 \cdot 10^{-11}$	0.30
D10v05H5	$1 \cdot 10^{-10}$	2.5	2.5	0.50	0.16	$3.04 \cdot 10^{-11}$	0.30
D10v05H6	$1 \cdot 10^{-10}$	2.5	3.1	0.62	0.24	$3.14 \cdot 10^{-11}$	0.31
D10v1H3	$1 \cdot 10^{-10}$	5.0	1.3	0.27	0.09	$3.06 \cdot 10^{-11}$	0.31
D10v1H4	$1 \cdot 10^{-10}$	5.0	1.9	0.38	0.18	$2.98 \cdot 10^{-11}$	0.30
D10v1H5	$1 \cdot 10^{-10}$	5.0	2.5	0.50	0.32	$3.01 \cdot 10^{-11}$	0.30
D10v1H6	$1 \cdot 10^{-10}$	5.0	3.1	0.62	0.47	$3.14 \cdot 10^{-11}$	0.31
D10v2H3	$1 \cdot 10^{-10}$	10.0	1.3	0.27	0.18	$3.05 \cdot 10^{-11}$	0.30
D10v2H4	$1 \cdot 10^{-10}$	10.0	1.9	0.38	0.36	$2.97 \cdot 10^{-11}$	0.30
D10v2H5	$1 \cdot 10^{-10}$	10.0	2.5	0.50	0.63	$3.03 \cdot 10^{-11}$	0.30
D10v2H6	$1 \cdot 10^{-10}$	10.0	3.1	0.62	0.95	$3.21 \cdot 10^{-11}$	0.32
D11v05H3	$1 \cdot 10^{-11}$	2.5	1.3	0.27	0.45	$3.59 \cdot 10^{-12}$	0.36
D11v05H4	$1 \cdot 10^{-11}$	2.5	1.9	0.38	0.90	$3.81 \cdot 10^{-12}$	0.38
D11v05H5	$1 \cdot 10^{-11}$	2.5	2.5	0.50	1.58	$4.21 \cdot 10^{-12}$	0.42
D11v05H6	$1 \cdot 10^{-11}$	2.5	3.1	0.62	2.37	$4.46 \cdot 10^{-12}$	0.45
D11v1H3	$1 \cdot 10^{-11}$	5.0	1.3	0.27	0.89	$3.57 \cdot 10^{-12}$	0.36
D11v1H4	$1 \cdot 10^{-11}$	5.0	1.9	0.38	1.79	$3.88 \cdot 10^{-12}$	0.39
D11v1H5	$1 \cdot 10^{-11}$	5.0	2.5	0.50	3.16	$4.41 \cdot 10^{-12}$	0.44
D11v1H6	$1 \cdot 10^{-11}$	5.0	3.1	0.62	4.75	$4.92 \cdot 10^{-12}$	0.49
D11v2H3	$1 \cdot 10^{-11}$	10.0	1.3	0.27	1.79	$3.77 \cdot 10^{-12}$	0.38
D11v2H4	$1 \cdot 10^{-11}$	10.0	1.9	0.38	3.59	$4.00 \cdot 10^{-12}$	0.40
D11v2H5	$1 \cdot 10^{-11}$	10.0	2.5	0.50	6.32	$4.52 \cdot 10^{-12}$	0.45
D11v2H6	$1 \cdot 10^{-11}$	10.0	3.1	0.62	9.50	$5.21 \cdot 10^{-12}$	0.52
D12v2H3	$1 \cdot 10^{-12}$	10.0	1.3	0.27	17.88	$5.31 \cdot 10^{-13}$	0.53
D12v2H4	$1 \cdot 10^{-12}$	10.0	1.9	0.38	35.87	$5.75 \cdot 10^{-13}$	0.58
D12v2H5	$1 \cdot 10^{-12}$	10.0	2.5	0.50	63.15	$6.94 \cdot 10^{-13}$	0.69
D12v2H6	$1 \cdot 10^{-12}$	10.0	3.1	0.62	94.99	$8.58 \cdot 10^{-13}$	0.86
D11v10H3	$1 \cdot 10^{-11}$	50.0	1.3	0.27	8.94	$3.90 \cdot 10^{-12}$	0.39
D11v10H4	$1 \cdot 10^{-11}$	50.0	1.9	0.38	17.94	$4.41 \cdot 10^{-12}$	0.44
D11v10H5	$1 \cdot 10^{-11}$	50.0	2.5	0.50	31.58	$5.27 \cdot 10^{-12}$	0.53
D11v10H6	$1 \cdot 10^{-11}$	50.0	3.1	0.62	47.49	$6.33 \cdot 10^{-12}$	0.63
D10v0H3	$1 \cdot 10^{-10}$	0.0	1.3	0.27	0.00	$3.12 \cdot 10^{-11}$	0.31
D10v0H4	$1 \cdot 10^{-10}$	0.0	1.9	0.38	0.00	$3.06 \cdot 10^{-11}$	0.31
D10v0H5	$1 \cdot 10^{-10}$	0.0	2.5	0.50	0.00	$3.06 \cdot 10^{-11}$	0.31
D10v0H6	$1 \cdot 10^{-10}$	0.0	3.1	0.62	0.00	$3.17 \cdot 10^{-11}$	0.32
D11v0H3	$1 \cdot 10^{-11}$	0.0	1.3	0.27	0.00	$3.61 \cdot 10^{-12}$	0.36
D11v0H4	$1 \cdot 10^{-11}$	0.0	1.9	0.38	0.00	$3.71 \cdot 10^{-12}$	0.37
D11v0H5	$1 \cdot 10^{-11}$	0.0	2.5	0.50	0.00	$3.86 \cdot 10^{-12}$	0.39
D11v0H6	$1 \cdot 10^{-11}$	0.0	3.1	0.62	0.00	$3.99 \cdot 10^{-12}$	0.40
D12v0H3	$1 \cdot 10^{-12}$	0.0	1.3	0.27	0.00	$6.38 \cdot 10^{-13}$	0.64
D12v0H4	$1 \cdot 10^{-12}$	0.0	1.9	0.38	0.00	$6.53 \cdot 10^{-13}$	0.65
D12v0H5	$1 \cdot 10^{-12}$	0.0	2.5	0.50	0.00	$6.48 \cdot 10^{-13}$	0.65
D12v0H6	$1 \cdot 10^{-12}$	0.0	3.1	0.62	0.00	$6.32 \cdot 10^{-13}$	0.63
D12v10H3	$1 \cdot 10^{-12}$	50.0	1.3	0.27	89.38	$7.65 \cdot 10^{-13}$	0.76
D12v10H4	$1 \cdot 10^{-12}$	50.0	1.9	0.38	179.36	$9.10 \cdot 10^{-13}$	0.91
D12v10H5	$1 \cdot 10^{-12}$	50.0	2.5	0.50	315.76	$1.17 \cdot 10^{-12}$	1.17
D12v10H6	$1 \cdot 10^{-12}$	50.0	3.1	0.62	474.94	$1.67 \cdot 10^{-12}$	1.67
D10v10H3	$1 \cdot 10^{-10}$	50.0	1.3	0.27	0.89	$3.36 \cdot 10^{-11}$	0.34
D10v10H4	$1 \cdot 10^{-10}$	50.0	1.9	0.38	1.79	$3.61 \cdot 10^{-11}$	0.36
D10v10H5	$1 \cdot 10^{-10}$	50.0	2.5	0.50	3.16	$3.97 \cdot 10^{-11}$	0.40
D10v10H6	$1 \cdot 10^{-10}$	50.0	3.1	0.62	4.75	$4.22 \cdot 10^{-11}$	0.42
D10v5H3	$1 \cdot 10^{-10}$	25.0	1.3	0.27	0.45	$3.05 \cdot 10^{-11}$	0.30
D10v5H4	$1 \cdot 10^{-10}$	25.0	1.9	0.38	0.90	$3.10 \cdot 10^{-11}$	0.31
D10v5H5	$1 \cdot 10^{-10}$	25.0	2.5	0.50	1.58	$3.36 \cdot 10^{-11}$	0.34
D10v5H6	$1 \cdot 10^{-10}$	25.0	3.1	0.62	2.37	$3.61 \cdot 10^{-11}$	0.36

233 4.1 Metachronal wave and velocity profiles

234 The focus of this article is on mass transfer, but, since convection, which depends on the local
235 velocity pattern, is an important means of mass transfer, in this section, we discuss the typical
236 velocity profiles obtained from the simulations. Fig. 5a shows the shape of the *metachronal*
237 *wave* obtained in the simulations by using the ‘ghost parabola’ approach. Concerning the
238 velocity profile (Fig. 5b), the most important feature for convective mass transport is the large
239 recirculation region occurring where the cilia bend. Higher velocities appear in other regions,
240 but these are confined within adjacent cilia and, as explained in Section 4.2, they do not
241 significantly increase mixing in the ciliated-layer. The penetration of the cilia in the mucus
242 layer is approximately $0.5\ \mu\text{m}$, which is consistent with values in the literature [22]. The
243 velocity of the mucus layer in our calculations is around $10\ \mu\text{m s}^{-1}$, which is consistent with
244 the values reported in the literature (typically ranging from $10 - 60\ \mu\text{m s}^{-1}$ [30]).

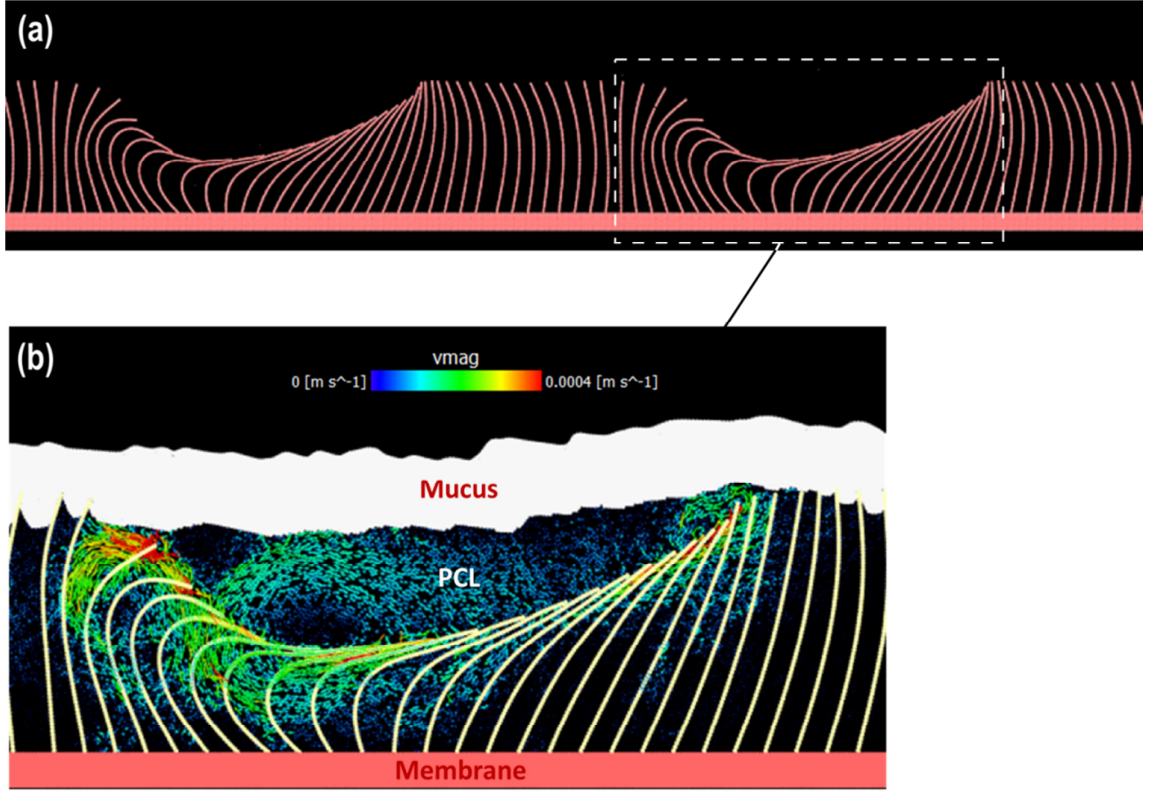
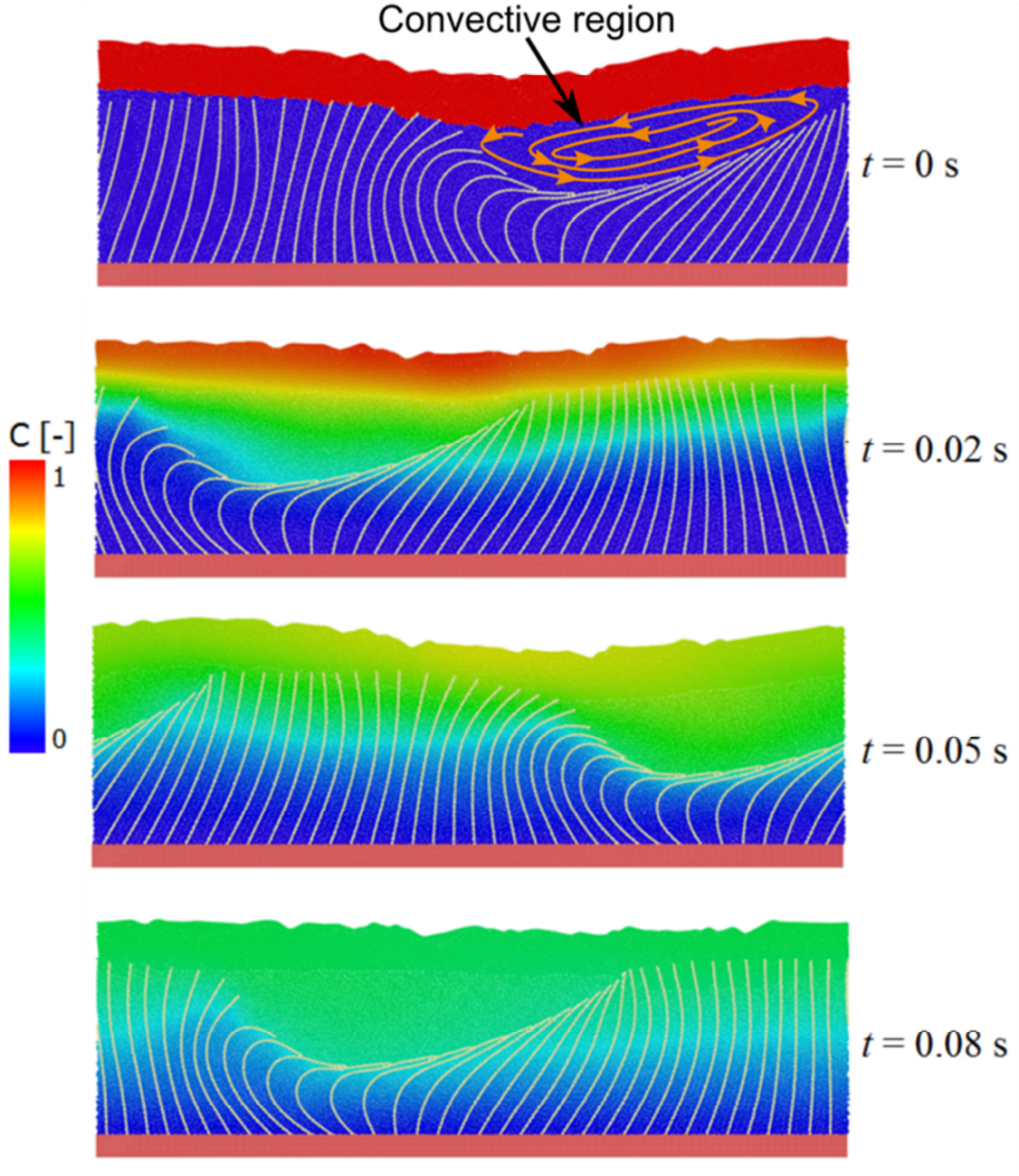


Fig. 5. *Metachronal wave* (a) and velocity profiles (b) for $D = 10^{-11} \text{ m}^2 \text{ s}^{-1}$, $f = 10 \text{ Hz}$, $s = 2.5 \text{ }\mu\text{m}$.

4.2 Concentration profiles

In order to study the mass transfer within the PCL, we include in our model the equation of mass conservation of a chemical species A. How this is introduced in the discrete multi-physics model is explained in Appendix D (additional details are given in [13]). A typical concentration profile is shown in Fig. 6.



252

253 Fig. 6. Concentration profiles of the chemical species A at different time steps ($D = 10^{-11} \text{ m}^2$
 254 s^{-1} , $f = 10 \text{ Hz}$, $s = 2.5 \text{ }\mu\text{m}$).

255 As the *metachronal wave* moves in the PCL, the bending of the cilia generates an empty
 256 region (free of cilia), called ‘convective region’ in Fig. 6, with characteristic size s , below the

257 mucus layer. This region has a large recirculation pattern that increases convective mass
 258 transport. Fig. 6 shows the effect of convection on a typical concentration profile. Initially, we
 259 assume all the drug is fully dissolved in the mucus layer and diffused in the PCL layer from
 260 there. The initial (dimensionless) drug concentration, therefore, is zero in the PCL and 1 in the
 261 mucus layer. The diffusivity of the drug is arbitrarily considered 10 times faster in the mucus
 262 than in the PCL, while the membrane is considered a passive wall with no mass exchange
 263 with the PCL. These boundary conditions allow for an effective calculation of D_{pcl} as
 264 explained in the next section.

265 4.3 Calculation of D_{pcl}

266 In order to calculate D_{pcl} , we need the instantaneous concentration profiles in the y -direction,
 267 which are calculated by averaging the concentration over the x -coordinate (Fig. 7a). Mass
 268 transfer in the PCL depends on a combination of diffusion and convection, however, under
 269 certain conditions the dynamics can be considered pseudo-diffusive and an apparent
 270 diffusivity coefficient D_{pcl} can be used to model mass transport in the ciliated-layer. We also
 271 assume that diffusivity of the drug is substantially larger in the PCL than in the membrane and
 272 we stop our simulation before the drug reaches the membrane. The usefulness of these
 273 assumptions can be understood from Eq. (3) and Fig. 3. From our simulations, we can only
 274 measure the total permeability P_{TOT} of the system. However, we want to calculate the
 275 permeability of the ciliated layer P_{pcl} . If we arbitrarily set the permeability in the mucus high,
 276 $1/P_{mu}$ in Eq. (3) can be neglected and, if we stop the simulation before the drug reaches the
 277 membrane, $1/P_{me}$ can neglect. Under these circumstances, therefore, $P_{TOT} \sim P_{pcl}$ and, by
 278 measuring P_{TOT} we estimate P_{pcl} . This is a sort of numerical ‘trick’, it has nothing to do with
 279 the real drug diffusion in the mucus, but allows to correctly estimate P_{pcl} . Once P_{pcl} is known,

280 realistic values of P_{TOT} can be calculated from Eq. (3) by introducing the actual values of P_{me}
281 and P_{mu} .

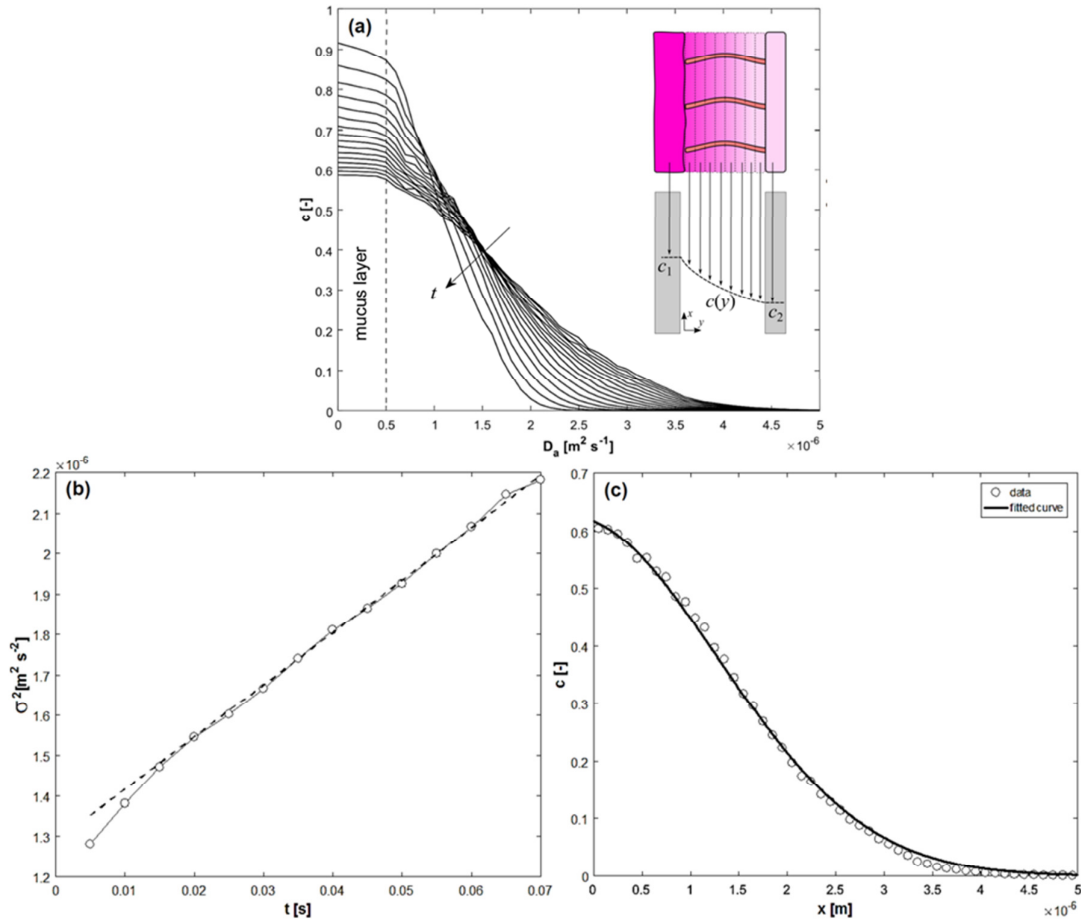
282 Under the assumptions discussed above, the time-dependent concentration profiles in the PCL
283 follow the formula [31]

$$c = c_{max} e^{-\frac{y^2}{4D_{pcl}t}}, \quad (11)$$

284 where c_{max} is the (time-dependent) concentration at $y = 0$, which depends on the total mass of
285 drug dissolved in the mucus at the beginning of the simulation and decays with time as $t^{0.5}$.

286

287



288

289 Fig. 7. Instantaneous concentration profiles in the y-direction (a), variance of the
 290 concentration versus time (b) and Gaussian fitting of the concentration profile at $t = 0.08$ s (c)
 291 for the case $D = 10^{-11} \text{ m}^2 \text{ s}^{-1}$, $f = 10 \text{ Hz}$, $s = 2.5 \text{ } \mu\text{m}$.

292 Given Eq. (11), we can calculate the value of D_{pcl} from the concentration profiles of Fig. 7a.
 293 We compute the (time-dependent) variance σ^2 of each concentration profile, which, if the
 294 assumptions behind Eq. (11) are valid, should change linearly with time (Fig. 7b). The slope
 295 of Fig. 7b, therefore, gives the numerical value of D_{pcl} . The pseudo-diffusive hypothesis
 296 implies that the concentration profiles are approximately Gaussian, this is verified in Fig. 7c
 297 for the specific case of $D = 10^{-11} \text{ m}^2 \text{ s}^{-1}$, $f = 10 \text{ Hz}$, $s = 2.5 \text{ } \mu\text{m}$. The same procedure for the

298 calculation of D_{pcl} is used for all the cases calculated in Table 1 and the results discussed in
299 the following sections.

300 4.4 Shielding

301 Fig. 8 shows how the Sherwood number changes with f and s in the case of $D = 10^{-11} \text{ m}^2 \text{ s}^{-1}$.
302 $Sh < 1$ implies that the pseudo-diffusivity in the PCL is lower than the drug's molecular
303 diffusivity. This behaviour may look surprising at a first glance since convection can only
304 increase mixing and, therefore, it is not clear how the pseudo-diffusivity of the PCL can be
305 lower than the drug's molecular diffusivity.

306 The presence of the cilia, however, creates obstacles to the free motion of the drug in the fluid
307 and, therefore, reduces the apparent mass transfer in the PCL. We have named this
308 phenomenon shielding and indicate with D_{0pcl} the lowest apparent diffusivity, which occurs at
309 $f \rightarrow 0$ where no convective mixing is present. As f increases, the convective motion enhances
310 mass transfer and compensates the shielding effect as discussed in the next section

311

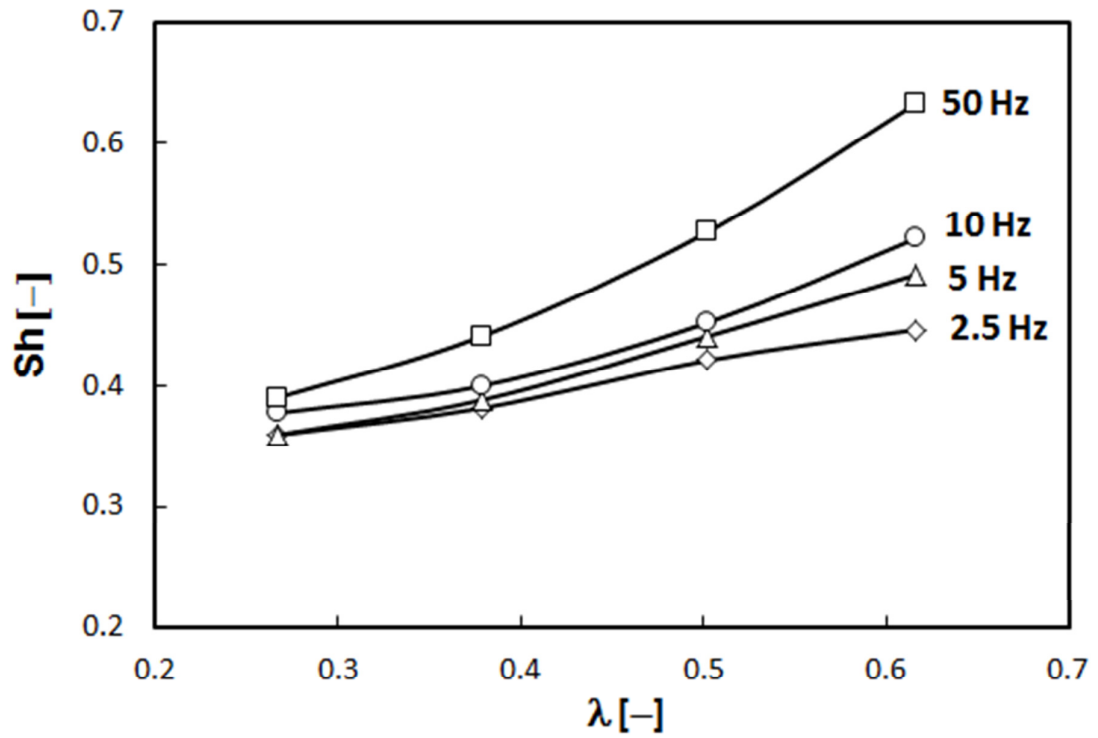


Fig. 8. Sherwood number for $D = 10^{-11} \text{ m}^2 \text{ s}^{-1}$ and various values of f and λ .

4.5 Mass transfer regimes

In Fig. 9 (Sh vs. Pe), we can distinguish three regions. Each of these regions is characterized by different values of K and n in Eq. (9). We are interested, in particular, in the exponent n and, therefore, we rewrite Eq. (9) as

$$D_{PCL} \propto s^{2n} f^n D^{1-n}. \quad (12)$$

Each value of n can be associate to a different mass transfer dynamics.

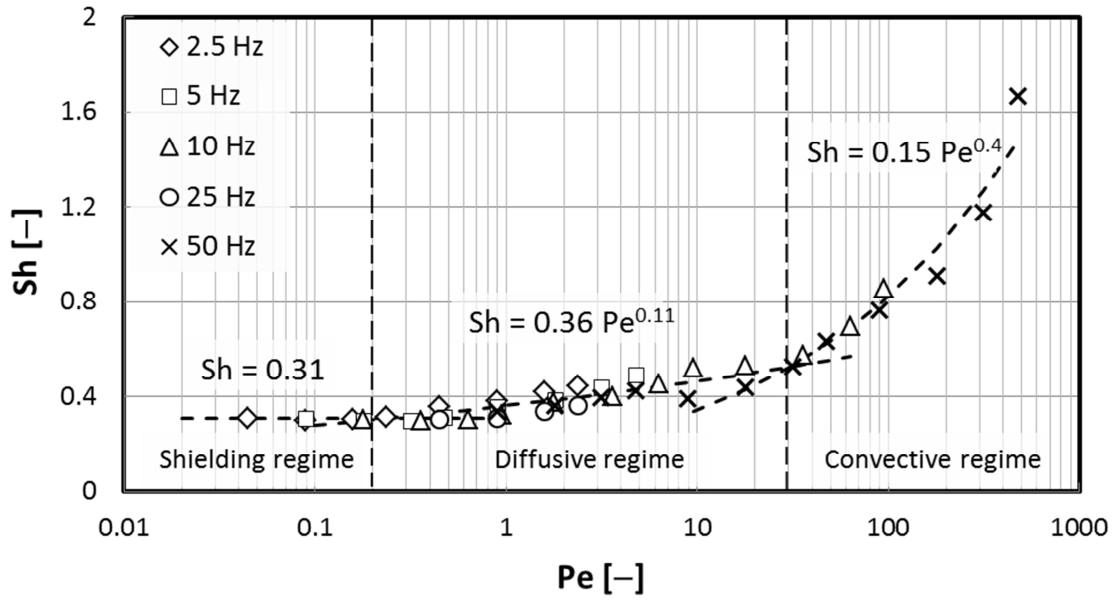


Fig. 9. Sherwood number versus Peclet number for all the simulations in Table 1.

Shielding regime ($Pe < 0.2$): the beat frequency is low and the shielding effect prevails. The mass transfer only depends on the diffusivity since the frequency of the cilia beat is very slow, but the pseudo-diffusivity is only one-third of the molecular diffusivity due to the shielding effect. The value 0.31 would probably change in three-dimensional simulations, but the general principle would remain valid. Considering Eq. (12) with $n = 0$,

$$D_{pcl} \propto D, \quad (13)$$

which confirms that the pseudo-diffusivity is proportional to the molecular diffusivity.

Diffusive regime ($0.2 < Pe < 30$): the cilia beat begins to ‘open’ the structure and allow higher mass transfer in the ciliated-layer. Sh increases, but shielding is still high ($Sh < 1$).

Considering Eq. (12) with $n = 0.1$,

$$D_{pcl} \propto s^{0.2} f^{0.1} D^{0.9}, \quad (14)$$

330 which shows that diffusion is still the main mass transfer mechanics as, in Eq. (14), D has the
 331 highest exponent.

332 Convective regime ($Pe > 0.3$): the cilia beat creates significant recirculation regions that
 333 increase Sh . Considering Eq. (12) with $n = 0.4$,

$$D_{pcl} \propto s^{0.8} f^{0.4} D^{0.6}, \quad (15)$$

334 which indicates that the role of the frequency becomes more significant (its exponent is now
 335 0.4). However, Eq. (15) also suggests that the size of the recirculation region (the exponent of
 336 s is 0.8) is even more important than the actual frequency.

337

338 **5. Conclusions**

339 In this paper, we have used the discrete multi-physics approach to simulate diffusive and
340 convective mass transfer in boundary layers containing motile cilia. Fluids (mucus and PCL)
341 and static solid (membrane) are implemented with the Smoothed Particle Hydrodynamics
342 while flexible cilia are structured with the Mass-Spring model.

343 *Metachronal wave* is mimicked by means of “ghost parabola” particles and a mass transfer
344 algorithm is introduced for modelling concentration diffusion between the mucus and the
345 membrane through the PCL.

346 The aim of the present study is to quantify the effects of the ciliated layers on the PCL flow
347 (convection) and mass transfer. Specifically, we have examined the role of the cilia beat
348 frequency, the flexibility of the cilia and the initial diffusivity of the mucus.

349 The aim of the present study is to quantify the effects of the ciliated layers on the PCL flow
350 (convection) and mass transfer. Specifically, we have examined the role of the cilia beat
351 frequency, the flexibility of the cilia and the initial diffusivity of the mucus. The model
352 accounts for several simplifications (2D geometry) and some of the complexities of the
353 biological system are neglected. In particular, it does not account for microvilli above the
354 ciliated cells, for discontinuities in the mucus layer and for presence of not-ciliated cells (e.g.
355 goblet cells). We believe that these factors can potentially affect mass transfer in the ciliated
356 layer to a certain degree. The physics behind the three mass transfer regimes (e.g. shielding,
357 diffusive and convective), however, is expected to remain the same.

358 Mass transfer in the ciliated-layer is hindered by the presence of cilia and the apparent
359 diffusivity reduces to one-third of the molecular diffusivity. As the frequency of the cilia beat

360 increases, recirculation regions appear in the velocity profile. In these regions, mass transfer
361 increases due to convective mixing. However, the size of the convective regions seems to
362 affect mass transfer more than the actual frequency. As a consequence of this, we suggest the
363 possibility that the capacity of the respiratory epithelium to absorb inhaled drugs may be more
364 strongly correlated with the flexibility of the cilia rather than the frequency of its beat. The
365 current results could also have implications for our understanding of the mechanisms that lead
366 to repeated infections and chronic respiratory syndrome in patients with ciliopathies. In
367 patients with primary pulmonary ciliary dyskinesia or the more common form of acquired
368 (secondary) ciliary dyskinesia the altered or completely suppressed function of the cilia
369 reduces the effectiveness of the mucociliary “conveyor belt”. As seen in this work, it also has
370 important implications on the speed with which both drugs and toxic agents can reach the
371 airway epithelium.

372 **Acknowledgements**

373 This article is based upon work from COST Action MP1404 SimInhale 'Simulation and
374 pharmaceutical technologies for advanced patient-tailored inhaled medicines', supported by
375 COST (European Cooperation in Science and Technology).

376 **Supporting Information**

377 A Appendix

378 B Appendix

379 C Appendix

380 D Appendix

381 REFERENCES

- 382 [1] Agnew JE, Sutton PP, Pavia D, Clarke SW. Radioaerosol assessment of mucociliary clearance -
383 towards definition of a normal range. *British Journal of Radiology*. 1986;59:147-51.
- 384 [2] Smith DJ, Gaffney EA, Blake JR. Modelling mucociliary clearance. *Respiratory Physiology &*
385 *Neurobiology*. 2008;163:178-88.
- 386 [3] Barton C, Raynor S. Analytical investigation of cilia induced mucous flow. *Bulletin of Mathematical*
387 *Biophysics*. 1967;29:419-&.
- 388 [4] Blake JR. Mechanics of Muco-ciliary Transport. *IMA Journal of Applied Mathematics*. 1984;32:69-
389 87.
- 390 [5] Mauroy B, Fausser C, Pelca D, Merckx J, Flaud P. Toward the modeling of mucus draining from the
391 human lung: role of the geometry of the airway tree. *Physical biology*. 2011;8:056006.
- 392 [6] Lee WL, Jayathilake PG, Tan ZJ, Le DV, Lee HP, Khoo BC. Muco-ciliary transport: Effect of mucus
393 viscosity, cilia beat frequency and cilia density. *Computers & Fluids*. 2011;49:214-21.
- 394 [7] Jayathilake PG, Tan Z, Le DV, Lee HP, Khoo BC. Three-dimensional numerical simulations of human
395 pulmonary cilia in the periciliary liquid layer by the immersed boundary method. *Computers & Fluids*.
396 2012;67:130-7.
- 397 [8] Jayathilake PG, Le DV, Tan Z, Lee HP, Khoo BC. A numerical study of muco-ciliary transport under
398 the condition of diseased cilia. *Comput Methods Biomech Biomed Engin*. 2015;18:944-51.
- 399 [9] Sedaghat MH, Shahmardan MM, Norouzi M, Jayathilake PG, Nazari M. Numerical simulation of
400 muco-ciliary clearance: immersed boundary lattice Boltzmann method. *Computers & Fluids*.
401 2016;131:91-101.
- 402 [10] Chatelin R, Anne-Archard D, Murriss-Espin M, Thiriet M, Poncet P. Numerical and experimental
403 investigation of mucociliary clearance breakdown in cystic fibrosis. *Journal of Biomechanics*.
404 2017;53:56-63.
- 405 [11] Olsson B, Bondesson E, Borgstrom L, Edsbacker S, Eirefelt S, Ekelund K, et al. Pulmonary Drug
406 Metabolism, Clearance, and Absorption. In: Smyth HDC, Hickey AJ, editors. *Controlled Pulmonary*
407 *Drug Delivery* 2011. p. 21-50.
- 408 [12] Alexiadis A. A smoothed particle hydrodynamics and coarse-grained molecular dynamics hybrid
409 technique for modelling elastic particles and breakable capsules under various flow conditions.
410 *International Journal for Numerical Methods in Engineering*. 2014;100:713-9.
- 411 [13] Alexiadis A. The Discrete Multi-Hybrid System for the Simulation of Solid-Liquid Flows. *Plos One*.
412 2015;10.
- 413 [14] Alexiadis A. A new framework for modelling the dynamics and the breakage of capsules, vesicles
414 and cells in fluid flow. In: BarthesBiesel D, Blyth MG, Salsac AV, editors. *Iutam Symposium on*
415 *Dynamics of Capsules, Vesicles and Cells in Flow* 2015. p. 80-8.

416 [15] Alexiadis A, Stamatopoulos K, Wen W, Batchelor HK, Bakalis S, Barigou M, et al. Using discrete
 417 multi-physics for detailed exploration of hydrodynamics in an in vitro colon system. *Computers in*
 418 *Biology and Medicine*. 2017;81:188-98.

419 [16] Ariane M, Allouche MH, Bussone M, Giacosa F, Bernard F, Barigou M, et al. Discrete multi-
 420 physics: A mesh-free model of blood flow in flexible biological valve including solid aggregate
 421 formation. *Plos One*. 2017;12.

422 [17] Ariane M, Wen W, Vigolo D, Brill A, Nash FGB, Barigou M, et al. Modelling and simulation of flow
 423 and agglomeration in deep veins valves using discrete multi physics. *Computers in Biology and*
 424 *Medicine*. 2017;96-103.

425 [18] Leopold PL, O'Mahony MJ, Lian XJ, Tilley AE, Harvey BG, Crystal RG. Smoking Is Associated with
 426 Shortened Airway Cilia. *Plos One*. 2009;4.

427 [19] Boucher RC. Airway surface dehydration in cystic fibrosis: Pathogenesis and therapy. *Annual*
 428 *Review of Medicine*2007. p. 157-70.

429 [20] Wang Y, Gao Y, Wyss HM, Anderson PD, den Toonder MJM. Artificial cilia fabricated using
 430 magnetic fiber drawing generate substantial fluid flow. *Microfluidics and Nanofluidics*. 2015;18:167-
 431 74.

432 [21] Aiello E, Sleight M. Ciliary function of the frog oro-pharyngeal epithelium. *Cell and Tissue*
 433 *Research*. 1977;178:267-78.

434 [22] Sanderson MJ, Sleight MA. Ciliary activity of cultured rabbit tracheal epithelium - beat pattern
 435 and metachrony. *Journal of Cell Science*. 1981;47:331-47.

436 [23] Marino MR, Aiello E. Cinemicrographic analysis of beat dynamics of human respiratory cilia. *J*
 437 *Progress in clinical and biological research*. 1982;80:35-9.

438 [24] Gheber L, Priel Z. Extraction of cilium beat parameters by the combined application of
 439 photoelectric measurements and computer simulation. *Biophysical Journal*. 1997;72:449-62.

440 [25] Chilvers MA, O'Callaghan C. Analysis of ciliary beat pattern and beat frequency using digital high
 441 speed imaging: comparison with the photomultiplier and photodiode methods. *Thorax*. 2000;55:314-
 442 7.

443 [26] Chilvers MA, Rutman A, O'Callaghan C. Functional analysis of cilia and ciliated epithelial
 444 ultrastructure in healthy children and young adults. *Thorax*. 2003;58:333-8.

445 [27] Chilvers MA, Rutman A, O'Callaghan C. Ciliary beat pattern is associated with specific
 446 ultrastructural defects in primary ciliary dyskinesia. *Journal of Allergy and Clinical Immunology*.
 447 2003;112:518-24.

448 [28] Fahrni F, Prins MWJ, van Ijzendoorn LJ. Micro-fluidic actuation using magnetic artificial cilia. *Lab*
 449 *on a Chip*. 2009;9:3413-21.

450 [29] Eixarch H, Haltner-Ukomadu E, Beisswenger C, Bock U. Drug Delivery to the Lung: Permeability
 451 and Physicochemical Characteristics of Drugs as the Basis for a Pulmonary Biopharmaceutical
 452 Classification System (pBCS). *Journal of Epithelial Biology & Pharmacology*. 2010;3:1-14.

453 [30] Oldenburg AL, Chhetri RK, Hill DB, Button B. Monitoring airway mucus flow and ciliary activity
454 with optical coherence tomography. Biomedical Optics Express. 2012;3:1978-92.

455 [31] Bird R, B., Stewart W, E., Lightfoot E, N. Transport phenomena. John Wiley & Sons, Revised 2nd
456 Edition edition ed2007.

457

458

459 **Appendix A**

460 The DMP version used in this study links SPH and MSM. In this section, we provide a brief
461 introduction to these techniques and how they are coupled together.

462 *1. Smoothed Particle Hydrodynamics (SPH)*

463 The SPH equations of motion are obtained from the discrete approximations of the
464 Navier-Stokes equation at a set of points, which can be thought as particles characterized by
465 their own mass, velocity, pressure and density. The fundamental idea behind this
466 approximation lies in the identity

$$467 \quad f(\mathbf{r}) = \iiint f(\mathbf{r}') \delta(\mathbf{r} - \mathbf{r}') d\mathbf{r}', \quad (\text{A.1})$$

468 where $f(\mathbf{r})$ is a generic function defined over the volume V , the vector \mathbf{r} is a three-dimensional
469 point in V and $\delta(\mathbf{r})$ is the three-dimensional delta function. In the SPH formalism, the delta
470 function is approximated by a smoothing Lucy kernel W with characteristic width h
471 (smoothing length) such that

$$472 \quad \lim_{h \rightarrow 0} W(\mathbf{r}, h) = \delta(\mathbf{r}). \quad (\text{A.2})$$

473 This brings to the approximation

$$474 \quad f(\mathbf{r}) \approx \iiint f(\mathbf{r}') W(\mathbf{r} - \mathbf{r}', h) d\mathbf{r}', \quad (\text{A.3})$$

475 which can be discretised over a series of particles of mass $m = \rho(\mathbf{r}) d\mathbf{r}$ obtaining

$$476 \quad f(\mathbf{r}) \approx \sum_i \frac{m_i}{\rho_i} f(\mathbf{r}_i) W(\mathbf{r} - \mathbf{r}_i, h), \quad (\text{A.4})$$

477 where m_i and ρ_i are the mass and density of the i^{th} particle, and i ranges over all particles
478 within the smoothing kernel (i.e. $|\mathbf{r} - \mathbf{r}_i| < h$). Equation (A.4) represents the discrete

479 approximation of a generic continuous field and can be used to approximate the Navier-Stokes
 480 equation

$$481 \quad m_i \frac{dv_i}{dt} = \sum_j m_i m_j \left(\frac{P_i}{\rho_i^2} + \frac{P_j}{\rho_j^2} + \Pi_{i,j} \right) \nabla_i W_{i,j} + \mathbf{f}_i, \quad (\text{A.5})$$

482 where v_i is the velocity of particle i , $W_{i,j}$ means $W(\mathbf{r}_j - \mathbf{r}_i, h)$, ∇_i denotes the gradient of the
 483 kernel with respect of the coordinate r_i , P is the pressure, \mathbf{f}_i a volumetric body force, and $\Pi_{i,j}$
 484 introduces the viscous forces. Various expressions for the tensor $\Pi_{i,j}$ are available; here we
 485 use (Monaghan and Gingold 1983)

$$486 \quad \Pi_{i,j} = -\alpha h \frac{c}{\rho_{ij}} \frac{v_{ij} \mathbf{r}_{ij}}{r_{ij}^2 + b h^2}, \quad (\text{A.6})$$

487 where α is a parameter (~ 1) used to ensure the stability of the simulation, c is the artificial
 488 sound speed in the liquid and b is a constant introduced to avoid singularities in the case of
 489 very close particles ($b \approx 0.01$). The value of α depends on the specific type of simulation; in
 490 this study we use $\alpha = 1$ as done in previous studies (Ariane et al. 2017a).

491 In order to close Eq. A.5, an equation of state linking ρ and P is required. In this paper, we
 492 use Tait's equation

$$493 \quad P(\rho) = \frac{c_0 \rho_0}{7} \left[\left(\frac{\rho}{\rho_0} \right)^7 - 1 \right], \quad (\text{A.7})$$

494 where c_0 and ρ_0 are, respectively the sound speed and density at zero applied stress.

495

496

497 2. Mass-Spring modelling (MSM) / Coarse-Grained Molecular Dynamics (CGMD)

498 Molecular dynamics is a form of investigation where the motion and the interaction of a
 499 certain number of computational atoms or molecules are studied. In classical MD simulations
 500 atoms move according to the Newtonian equations of motion

$$501 \quad m_i \frac{dv_i}{dt} = -\frac{\partial}{\partial \mathbf{r}} U_{tot}(\mathbf{r}_1, \mathbf{r}_2, \dots, \mathbf{r}_N), \quad (\text{A.8})$$

502 where U_{tot} is the total interatomic potential, which can be divided into two main parts: non
 503 bonded and intramolecular. Non bonded forces are usually represented by the so-called
 504 Lennard-Jones potential, while the intramolecular forces are often divided in subgroups e.g.

$$505 \quad U_{intramolecular} = U_{bond} + U_{angle} \quad (\text{A.9})$$

506 Each of these potentials can have different forms. In this study, we use the harmonic bond
 507 potential

$$508 \quad U_{bond} = k_b (r - r_0)^2, \quad (\text{A.10})$$

509 where k_b a Hookean coefficient, r_0 the equilibrium distance, and the harmonic angle potential

$$510 \quad U_{angle} = k_a (\theta - \theta_0)^2, \quad (\text{A.11})$$

511 where k_a is an angular Hookean coefficient and θ_0 the equilibrium angle,

512 Equations (A.9–A.11) are the basis for the ball-and-stick representation of molecules that can
 513 be coarse-grained to model macroscopic solids within the MSM framework. This approach
 514 can be employed to model macroscopic phenomena such as stretching and bending of solids
 515 under the effect of external forces. In the case under investigation, we divide the membrane in
 516 a certain number of notional particles and use the potentials of Eq. A.10 and A.11 to simulate
 517 its deformation. Figure 1 shows how bond and angle potentials are used in the membrane

518 model. This component of the DMP has been indicated sometimes as MSM and sometimes as
 519 CGMD. The mathematical formulation is the same: at small scales (e.g. microfluidic
 520 applications) the term CGMD is preferred (Alexiadis 2014), at larger scales the term MSM is
 521 preferred (Alexiadis et al. 2017).

522 3. Coupling the two models

523 The interaction between the solid (MSM particles) and the liquid (SPH particles) is defined by
 524 boundary conditions, which relate the behaviour of two adjacent materials at the common
 525 interface. There are three main types of phenomena that must be taken into consideration in
 526 designing these boundary conditions (Müller et al. 2004): no-penetration, no-slip and
 527 continuity of stresses. In continuum mechanics, these conditions are often represented as

$$528 \quad \left(\frac{\partial}{\partial t} \mathbf{u} - \mathbf{v}\right) \cdot \mathbf{n} = \mathbf{0} \quad (\text{no - penetration}), \quad (\text{A.12})$$

$$529 \quad \left(\frac{\partial}{\partial t} \mathbf{u} - \mathbf{v}\right) \times \mathbf{n} = \mathbf{0} \quad (\text{no - slip}) \quad (\text{A.13})$$

530 and

$$531 \quad \sigma_s \mathbf{n} = \sigma_f (-\mathbf{n}) \quad (\text{continuity of stresses}) \quad (\text{A.14})$$

532 where \mathbf{n} is the normal to the boundary, \mathbf{u} the displacement of the solid, \mathbf{v} the velocity of the
 533 liquid, σ_s the stresses in the solid and σ_f in the fluid.

534 In the particle framework, various no-penetration methods can be implemented (Ferrand et al.
 535 2013) and an additional central force of the Lennard-Jones type is often used

$$536 \quad f(r) = K \left[\left(\frac{r^*}{r} \right)^{n_1} - \left(\frac{r^*}{r} \right)^{n_2} \right] \frac{1}{r^2}, \quad (\text{A.15})$$

537 where r^* represents the repulsive radius of the particle, and n_1 and n_2 are usually set to 4 and
538 2, although also the original 12-6 Lennard-Jones values are sometimes used. The constant K is
539 chosen on the basis of a characteristic velocity of the flow.

540 Concerning the “ghost parabola”, we use a softer repulsion potential based on a cosines form
541 that only push apart overlapping cilia particles

$$542 \quad f(r) = K_s \left[1 + \cos\left(\frac{\pi r}{r^*}\right) \right], \quad (\text{A.16})$$

543 With K_s a constant chosen arbitrarily according to the simulations.

544 The no-slip condition models the friction between the solid and the fluid. In finite-element
545 numerical methods it is enforced by imposing that the two materials have the same velocity at
546 the interface. The advantage of using a particle-particle representation is that, once both the
547 no-penetration and no-slip boundary condition are enforced, the continuity of stress is
548 automatically satisfied by the equation of motion (A.5).

549 **References**

550 Ferrand, M., D. R. Laurence, B. D. Rogers, D. Violeau and C. Kassiotis (2013). "Unified
551 semi-analytical wall boundary conditions for inviscid, laminar or turbulent flows in the
552 meshless SPH method." *International Journal for Numerical Methods in Fluids* 71(4): 446-
553 472.

554 Monaghan, J. J. and R. A. Gingold (1983). "Shock simulation by the particle method SPH."
555 *Journal of Computational Physics* 52(2): 374-389.

556 Müller, M., S. Schirm, M. Teschner, B. Heidelberger and G. M (2004). "Interaction of fluids
557 with deformable solids." *Computer Animation and Virtual Worlds* 15: 159-171.

558

Appendix B

There are two types of parameter required for the simulations: model parameters and simulation parameters. Table B.1 list the numerical values used in the model parameters (simulation parameters are discussed in section 2 of the manuscript).

Table B.1. Model parameters used in the simulations.

SPH (eqs. A.5–A.7)	
Parameter	Value
Number of membrane particles (10 layers)	3270
Number of PCL particles	19788
Number of mucus particles N_{mucus}	7050
Number of cilium particles (36 cilia)	2592 (72 particles/cilium)
Number of Ghost parabola particles (1 layer)	343
Mass of each particle	$4.3 \cdot 10^{-12}$ kg
Initial distance among particles Δr	$6.6 \cdot 10^{-8}$ m
Smoothing length h	$1.98 \cdot 10^{-7}$ m
Artificial sound speed c_0	0.25 m s ⁻¹
Density of PCL ρ	1000 kg m ⁻³
Density of mucus ρ	1000 kg m ⁻³
Dynamic viscosity of PCL μ	$1 \cdot 10^{-3}$ Pa s
Dynamic viscosity of mucus μ	20 Pa s
Time step Δt	10^{-8} s
MSM (eqs. A.8-A.11)	
Parameter	Value
Angular coefficient k_a	$1.0 \cdot 10^{-12}$ J
Hookian coefficient k_b	20 J m ⁻²
Equilibrium distance r_0	$6.6 \cdot 10^{-8}$ m
BOUNDARIES (Eq. A12-A.15)	
Constant K	$5 \cdot 10^{-16}$ J
Constant Ks	$8 \cdot 10^{-15}$ J
Repulsive radius r^*	$1.65 \cdot 10^{-7}$ m

The viscoelastic properties of the mucus are discussed in Appendix C.

567 **Appendix C**

568 To model viscoelastic fluids in discrete multi-physics, we can implement the viscosity via
 569 SPH forces (see Appendix A) and add the elasticity as an equivalent attractive force

$$k_b = \frac{EA_0}{L_{mu}}, \quad (C.1)$$

570 where k_b is the Hookean bending coefficient of Eq. A.10, E the Young modulus of mucus, A_0
 571 the sectional area and L_{mu} the thickness of the mucus layer.

572 Moreover, since the elastic force is shared by all the mucus particles $k^*=k_b/N_{mucus}$, where
 573 N_{mucus} is the number of computational particles used for the mucus layer. Mucus is a
 574 viscoelastic fluid and not a viscoelastic solid, consequently, we cannot use actual Hookean
 575 springs that would prevent relative motion of the fluid particles. Therefore, we approximate
 576 locally the harmonic potential with a Lennard Jones form with the minimum in the same
 577 position. This implies that the second derivative of both potentials should be the same at r_0
 578 e.g.

$$\frac{dU_{LJ}}{dr^2} = \varepsilon \left[156 \frac{r_0^{12}}{r^{14}} - 84 \frac{r_0^6}{r^8} \right] = 72\varepsilon \text{ at } r = r_0, \quad (C.2)$$

579 which gives $\varepsilon = k^*/72$.

580 In our case, $E = 10$ Pa ; $N_{mucus} = 7050$, $L_{me} = 0.6 \cdot 10^{-6}$ m and, therefore, $\varepsilon = 1 \cdot 10^{-6}$ J. This
 581 produces a Maxwell viscoelastic material with $\mu = 20$ Pa s and $E = 10$ Pa.